Measurement of Internal Stress and Internal Resistance Resulting from Creep of Type 316H Stainless Steel

<u>Bo Chen</u>[1,*], David J. Smith[1], Peter E.J. Flewitt[2, 3], Shu Yan Zhang[4]

[1] Department of Mechanical Engineering, University of Bristol, Bristol BS8 1TR, UK
[2] Interface Analysis Centre, University of Bristol, 121 St. Michael's Hill, Bristol BS2 8BS, UK
[3] H.H. Wills Physics Laboratory, University of Bristol, Tyndall Avenue, Bristol BS8 1TL, UK
[4] ISIS, Science and Technology Facilities Council, Rutherford Appleton Laboratory, Chilton, Didcot OX11 0QX, UK
* Corresponding author: b.chen@bristol.ac.uk

Abstract   Descriptions of high temperature creep deformation often use the concept of the effective stress, which includes the presence of the internal stress.   Many experimental techniques have been applied to measure the internal stress induced by creep deformation.   However, there is still a debate about the validity of the measured values.   This is partly because the distinction between internal stress and material internal resistance is unclear.   In this paper, neutron diffraction measurements, undertaken using the spallation source at the Rutherford Appleton Laboratory, UK, are combined with in-situ loading to investigate the internal state of a Type 316H stainless steel.   By undertaking measurements of the lattice strain for different grain families, before, during and after mechanical loading, the internal stress and internal resistance induced by prior creep were determined.   The results show that these two parameters are important measures of the internal state, each changing during creep and influencing creep deformation rate.   Additionally, internal stress is shown to be dependent on specific crystallographic planes of each grain family.   The results are discussed with respect to the underlying mechanisms of creep deformation in stainless steel.

Keywords   Internal Stress, Internal Resistance, Creep, Neutron Diffraction, Austenitic Stainless Steel

1. Introduction

Materials may deform by one of several different mechanisms depending upon the applied stress and temperature.   It is convenient to present these mechanisms in the form of a deformation mechanism map [1].   More importantly, the use of engineering polycrystalline materials over the operational service life (typically $>10^5$ hours) produces a potential to change the initial microstructure, which can affect the controlling deformation mechanisms in creep [2, 3].   It has been recognised by Biberger and Gibeling [4] that creep deformation rate, $\dot{\varepsilon}_c$, relies on the state of the microstructure, temperature and applied stress.   Thus, the deformation rate is described by a kinetic equation of the form:

$$\dot{\varepsilon}_c = f(\sigma_a, T, \hat{\sigma}_1, \hat{\sigma}_2 \cdots \sigma_n) \tag{1}$$

where σ_a is the applied stress, T is the temperature, $\hat{\sigma}_1$, $\hat{\sigma}_2$ and $\hat{\sigma}_n$ represent a series of known and unknown internal state parameters which characterise the current state of the material.   In addition, creep deformation leads to changes to the internal state parameters.   Two of these parameters are considered here: (i) the creation of internal strains arising from strain incompatibility, for example due to the different creep deformation rates of individual grains in polycrystalline materials; (ii) a change in the material resistance.   The first is called as internal stress and the second is called as internal resistance, as described by Chen et al. [5].

Many experimental techniques have been developed to provide a quantitative measure of these two terms, such as the widely accepted stress dip test technique [6], analysis of asymmetric X-ray diffraction peak profiles [7], dislocation density and geometrical arrangement obtained using transmission electron microscopy (TEM) [8].   In addition, creep deformation models, incorporating the term internal stress or internal resistance, have been developed to improve the prediction in creep deformation rate.   These include models proposed by Estrin and Mecking [9],

Derby and Ashby [10], Esposito and Bonora [11]. However, there are two challenges remaining before those physically based creep deformation models can be adopted for the extension of life of existing power generation plants as well as the prediction of life for the future designs. First, the distinction between internal stress and internal resistance is often confusing and unclear [5]. Second, a reliable and simple measurement technique to quantify these two terms unambiguously is still required.

In this paper, we present a technique, based on neutron diffraction (ND) measurement combined with in-situ tensile deformation, to quantify the internal stress and internal resistance associated with high temperature creep deformation. The evolution of these two terms during creep deformation is measured quantitatively by this method. The crystallographic orientation dependence of the internal stress is discussed with respect to the underlying mechanisms of polycrystalline elasticity and plasticity. A newly developed self-consistent model has been established to interpret the measured results. The model is presented in the companion paper for this conference [12]. The ability of adopting this experimental technique to quantify internal state of the material is critically assessed, followed by concluding remarks.

2. Material and Experimental

2.1. Material

Type 316H austenitic stainless steel, provided by EDF Energy plc., with a chemical composition given in Table 1, was examined. The stainless steel had experienced 65,015 hours service at temperatures in the range of 763K to 803K and it was then subjected to a further thermal ageing at 823K for 22,100 hours. The grain size for this stainless steel was measured using the linear intercept method. The averaged grain size was 87±9μm.

Table 1. Chemical composition (wt.%) of Type 316H stainless steel

C	Si	Mn	P	S	Cr	Mo	Ni	Co	B	Fe
0.06	0.4	1.98	0.021	0.014	17.17	2.19	11.83	0.10	0.005	Bal.

Table 2. Summary of specimens subject to a prior deformation at high temperature (250MPa and 823K)

Specimen ID	Creep test duration	Plastic loading true strain, %	True creep strain, %
Specimen 1	No creep	0	0
Specimen 2	As loaded	1.88	0
Specimen 3	Primary, 160h	2.04	0.92
Specimen 4	Secondary, 1000h	1.98	4.86

2.2. Prior deformation at high temperature

To study systematically the influence of the prior deformation at high temperature on the internal state of the material, four prior deformation states were considered: (i) no creep, (ii) as loaded, (iii) primary creep, and (iv) secondary creep. Four specimens were prepared from the Type 316H austenitic stainless steel. Prior deformation tests at a temperature of 823K were then carried out. A summary is given in Table 2. Uniaxial round bar specimens with a 28.25mm gauge length and 5.65mm diameter were used. These specimens were deformed at 823K and at a constant stress of 250MPa to different stages of creep deformation. The left hand side in Fig. 1 (a) illustrates the strain history for a specimen, which was strained to reach primary creep. The specimen was heated to a temperature of 823K, step 1 in Fig. 1 (a). This was followed by the application of load

to reach the test stress of 250MPa at 823K, step 2 in Fig. 1 (a). Specimen was then creep deformed to a pre-defined creep duration, which was followed by cooling under the applied load to freeze the creep induced dislocation structure. Finally the specimen was unloaded and dismantled at room temperature. This procedure was adopted for each specimen shown in Table 2. Each specimen was then subject to incremental tensile deformation at room temperature and simultaneously measured using neutron diffraction. This is detailed in the next section.

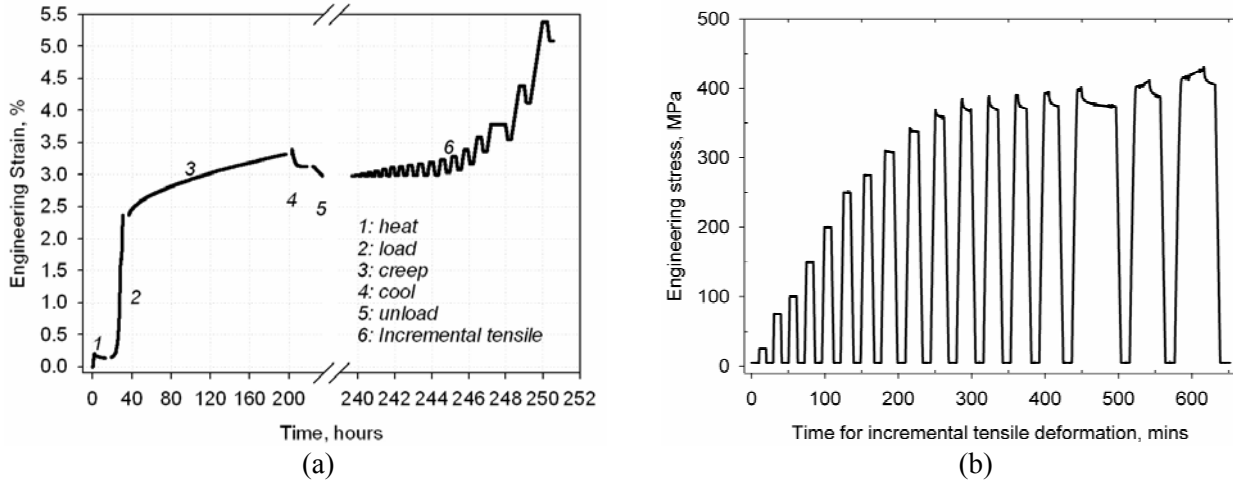(a)   (b)

Figure 1. A schematic diagram of the history applied to the specimen strained to the primary creep, followed by the room temperature incremental tensile deformation: (a) strain history and (b) stress cycles used in the incremental tensile deformation at room temperature combined with ND measurement

2.3. Incremental tensile deformation combined with neutron diffraction (ND)

The time-of-flight neutron diffractometer, at the Rutherford Appleton Laboratory, UK, is optimised to measure elastic strains at precise locations for the bulk material [13]. A pulsed beam of neutrons with a wide energy range travels to the specimen, see Fig. 2 (a), where a small fraction of the beam is diffracted to both detectors located at an angle of $2\theta = 90°$. This arrangement provides a measure of axial strain vector from detector 1 and radial strain vector from detector 2, Fig. 2 (a). The wavelength, λ, of the detected neutrons is defined from their time-of-flight, t.

$$\lambda = \frac{h}{m(L_1 + L_2)}t \qquad (2)$$

where h is the Planck constant, m is the neutron mass and L_1 and L_2 are the flight paths from the moderator to specimen and from the specimen to detector, respectively. A typical spectrum obtained from stainless steel is shown in Fig. 2 (b). Each diffraction peak, at a specific time-of-flight, according to Bragg's law, $\lambda_{hkl} = 2d_{hkl}\sin\theta$, represents a grain family with $\{hkl\}$ crystallographic orientation under a specific elastic strain. The evaluation of the elastic strain in each grain family of the material requires a measure of the lattice spacing of this grain family under the stress free condition. The elastic strain is determined from the change in the lattice spacing, as compared with the stress free lattice spacing:

$$\varepsilon_{hkl} = \frac{d_{hkl} - d_{hkl}^0}{d_{hkl}^0} \qquad (3)$$

where ε_{hkl} is the elastic strain in the $\{hkl\}$ grain family, d_{hkl} is the lattice spacing at a specific strain state and d_{hkl}^0 is the stress free lattice spacing. In this paper, four diffraction peaks are considered: $\{111\}$, $\{200\}$, $\{220\}$ and $\{311\}$ grain families, see Fig. 2 (b). In the time-of-flight instrument, the engineering strain can also be approximated from a Rietveld refinement of the

complete diffraction spectrum, see Fig. 2 (b) [13].   By knowing two principal strain vectors, the stress state in each grain family can be calculated from the generalized Hooke's law [14].   In our case, both axial and radial strain vectors have been measured from detectors 1 and 2.
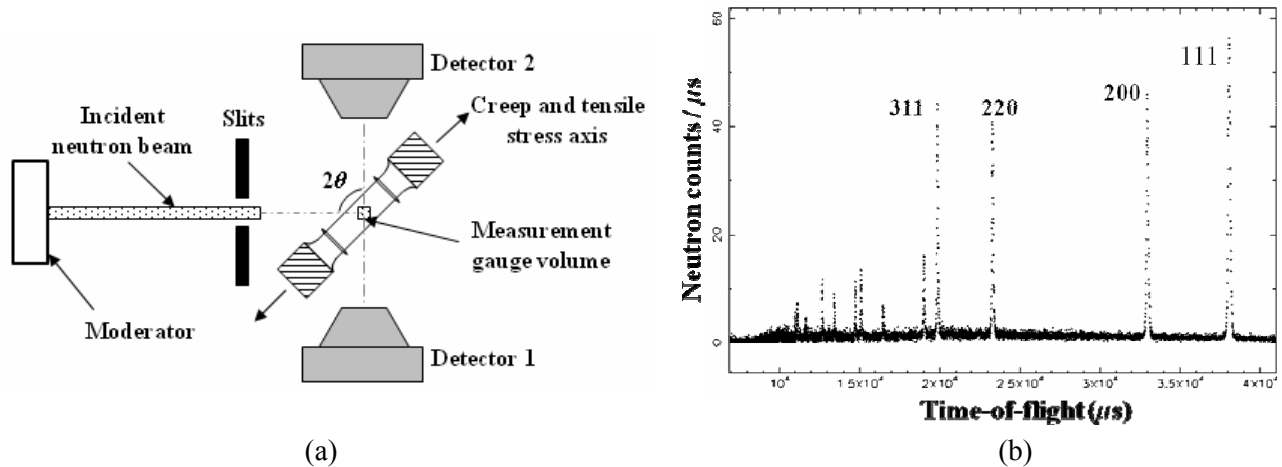

(a)   (b)

Figure 2. Neutron diffraction: (a) arrangement of the in-situ tensile deformation specimen in the ENGIN-X neutron diffractometer; (b) typical time-of-flight diffraction spectrum for the investigated stainless steel

In-situ tensile deformation was performed at room temperature on the specimens, which had been subjected to a prior deformation at high temperature, see Figs. 1 (a) and (b).   The arrangement of the neutron diffractometer in ENGIN-X with respect to the specimen is shown in Fig. 2 (a).   The direction of applied loading for the prior creep deformation and the direction of the incremental tensile deformation were co-axial.   As illustrated in Fig. 1 (a), room temperature incremental deformation may be considered to be a continuation of deformation in terms of the total strain accumulated.   Fig. 1 (b) shows the applied stress history during the incremental tensile deformation, where the stress level was increased step by step.   At the end of each load step, the specimen was held at either a constant stress (elastic region) or at a constant strain (plastic region) for the period of the neutron diffraction (ND) measurement time to provide a measure of d_{hkl}, see Figs. 1 (a) and (b)   All the incremental tensile deformation tests were undertaken at a constant strain rate of 5×10^{-6}/s using the ENGIN-X 100kN servo-hydraulic stress rig.   A fixed rate was selected because the yield point of stainless steel is very strain rate dependent.   An extensometer was attached onto the specimen to measure the bulk axial strain of the material during loading.

A 3mm×3mm×4mm gauge volume was used for the neutron diffraction (ND) measurements to ensure the sampled gauge volume was fully contained within the specimen, as illustrated schematically in Fig. 2 (a).   A typical measurement time of 540s was selected to ensure good counting statistics for the diffraction peaks.   Some stress relaxation was observed when the stress was higher than 300MPa, Fig. 1 (b).   To ensure the stress change was less than 3MPa when measurements were undertaken in the plastic region, a pre-defined delay for starting ND measurements, ranging from 180s to 360s, was adopted.   Therefore all the neutron diffraction measurements were undertaken at a relatively constant stress.

2.4. Derivation of internal stress and internal resistance due to creep

The internal stress, due to the prior deformation at high temperature, was quantified directly by the change in the lattice spacing which was measured from each specimen (without being subjected to the incremental tensile deformation).   Specimen 1 was not subjected to any prior deformation at high temperature, and therefore was considered to be a reference state that was free of internal

stress. The lattice spacings measured in the other three specimens, Table 2, were then compared with specimen 1:

$$\varepsilon_{hkl}^{i} = \frac{d_{hkl}^{i} - d_{hkl}^{1}}{d_{hkl}^{1}} \tag{4}$$

where ε_{hkl}^{i} is the internal strain in specimen i (i=1, 2, 3 or 4 based on Table 2), d_{hkl}^{1} is the lattice spacing in {hkl} plane measured from specimen 1 and d_{hkl}^{i} is the lattice spacing measured from specimen i (i=1, 2, 3 or 4 based on Table 2).

Internal resistance measurements were undertaken using a combination of loading and unloading steps to enhance the accuracy for the determination of the initial yield point in each specimen, Fig. 1 (b). In practice, the internal resistance is equal to the magnitude of applied stress that produced a deviation from linearity on a peak strain versus applied stress graph (ε_{hkl}-σ_a graph). The deviation from linearity was calculated from the difference between the measured elastic lattice strain and the predicted elastic lattice strain from diffraction elastic constants. It should be mentioned that the internal resistance measured using this method does not take into account the presence of internal stress. Thus the corrected internal resistance in each specimen was evaluated by deducting the magnitude of the pre-existing internal stress from the initially determined internal resistance.

A series of unloading steps to a nominally zero applied stress (5MPa) was adopted during the incremental tensile deformation, Fig. 1 (b). Using this approach it was possible to track the change in the internal stress introduced by room temperature tensile deformation. This can be then added to the pre-existing internal stress due to high temperature deformation to provide a measure of the evolution of internal stress introduced by the general plastic deformation, i.e. the sum of room temperature plastic deformation and high temperature plastic and creep deformations.

3. Results

3.1. Response of lattice strain responses and deviations from linearity

Fig. 3 (a) shows the ND measured lattice strains along the axial direction as a function of increasing applied stress for specimen 1, not subjected to a prior high temperature deformation. The diffraction elastic constants (DECs) for all four grain families were determined from the ND measurement data within the elastic region, the linear portion of the ε_{hkl}-σ_a graph, below the elastic limit illustrated by the dotted line in Fig. 3 (a).   A linear least squares regression method was used to fit the data and obtain the DECs.   From the region where the applied stress was above the elastic limit, the measured lattice strains for the {220}, {111} and {311} grain families diverged from linearity towards a lower strain value (to the left hand side of the prediction), whereas the {200} lattice strain diverged to a larger strain value (to the right hand side of the prediction).   Fig. 3 (b) shows the calculated difference between the ND measured lattice strain and the predicted lattice strain using the DEC for each grain family.   After reaching the applied stress of 375MPa, Fig. 3 (b), the difference was about -500×10^{-6} strain (compression) for the {220} grain family, however for the {200} grain family the difference was about +500×10^{-6} strain (tension).   In addition the bulk plastic strain measured by the extensometer provided a consistent prediction of the deviation from linearity, Fig. 3 (b).   This data analysis procedure was adopted for each specimen.   The DECs and elastic limits of all four specimens are summarised in Table 3.   Among the four grain families, {200} grain family was the most compliant and the {111} grain family was the stiffest. The progressive increase in the elastic limit from specimens 1 to 4 was consistent with the increase in the total strain introduced by the prior deformation at high temperature.   The uncertainty for the

determination of the DECs is also given in Table 3 for each grain family.

Fig. 4 (a) and (b) show the influence of prior deformation at high temperature on the response of the lattice strains to the applied stress for the {200} and the {220} grain families, respectively. They are illustrated by the deviation from linearity. A negative value indicates the presence of a micro-yielding in a particular grain family and a positive value indicates the effects of sharing load due to yielding of other grain families. The uncertainties shown in the Figs. 4 (a) and (b) are based on the uncertainties in the determination of DECs, summarised in Table 3. This applies to all specimens shown in Figs. 4 (a) and (b). In terms of the {200} grain family, Fig. 4 (a), the magnitude of the deviation from linearity (positive values), decreased to a minimum value from specimen 1 to specimen 3, but increased slightly for specimen 4. The deviation from linearity observed in specimen 3 was typically less than 100×10^6 and thus was less than the uncertainty. In terms of the {220} grain family, a very small decrease in the magnitude of the deviation from linearity (negative values) was observed from specimen 1 to specimen 3, Fig. 4 (b). However, specimen 4 showed a different lattice strain response, compared with the other three.

Table 3. Summary of diffraction elastic constants (DECs) and elastic limits of specimens

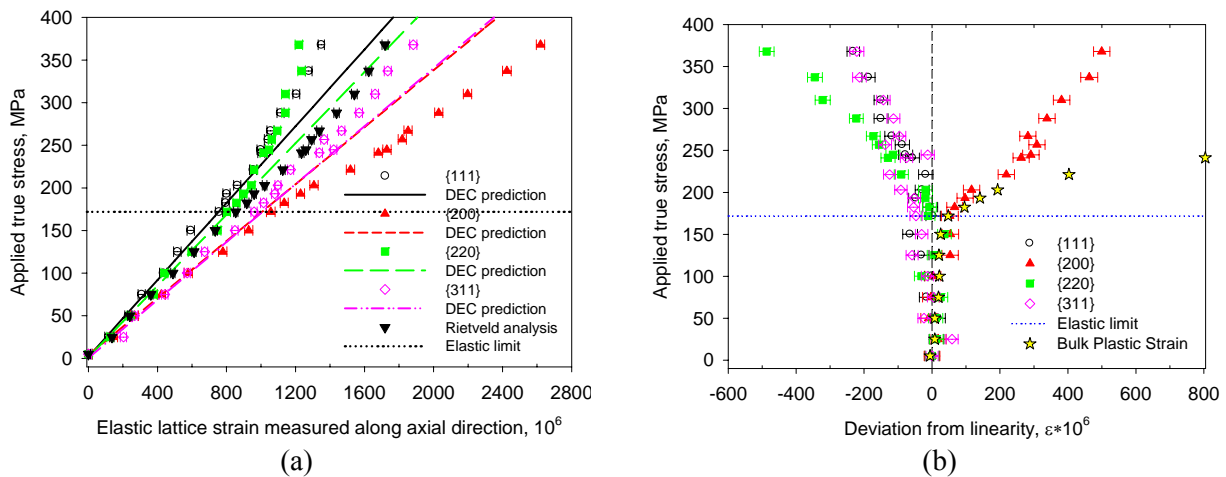| Specimen ID	Prior deformation	$E_{\{111\}}$, GPa	$E_{\{200\}}$, GPa	$E_{\{220\}}$, GPa	$E_{\{311\}}$, GPa	Elastic limit (measured at 0.01% bulk plastic strain), MPa
Specimen 1	No creep	225±12	167±5	209±16	170±16	184
Specimen 2	As loaded	255±21	155±4	211±8	172±8	333
Specimen 3	Primary	264±16	146±6	201±7	204±15	344
Specimen 4	Secondary	254±4	171±9	255±16	208±12	377
Averaged DECs		250±16	160±11	219±24	188±20	

Figure 3. (a) ND measured elastic lattice strain along the axial direction of specimen 1 for {111}, {200}, {220} and {311} grain families; (b) Deviation of the measured lattice strain from the extrapolated elastic lattice strain using DECs.   Note: Measurement uncertainties are from the single peak fitting error

Neutron diffraction measurements undertaken at 5MPa after each step of unloading over the process of incremental tensile deformation at room temperature, see Fig. 1 (b), revealed the evolution of the residual elastic lattice strain. Figs. 5 (a) and (b) show the changes in the residual lattice strains with the increase in the bulk plastic strain measured by the extensometer attached on the specimen, for the {200} and {220} grain families, respectively. In terms of the {200} grain family, specimen 4 which was subjected to prior secondary creep deformation, had the highest compressive residual lattice strain, but specimen 1 had the highest tensile residual lattice strain. In terms of the {220}

grain family, very little residual elastic lattice strain ($<150 \times 10^{-6}$ strain) was accumulated during incremental tensile deformation of specimens subjected to prior deformation at high temperature.

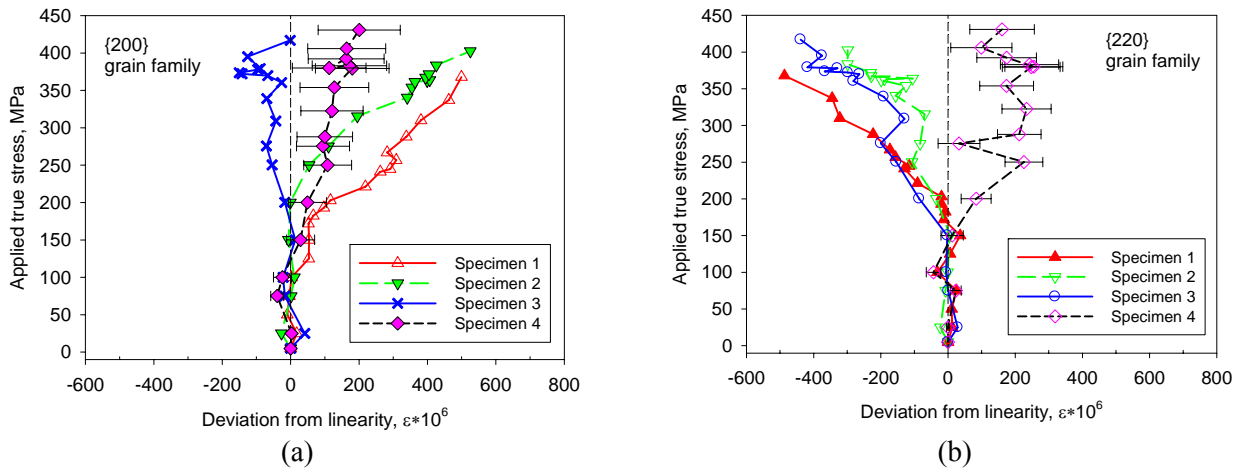(a)   (b)

Figure 4. Influence of prior deformation at high temperature on the subsequent elastic lattice strain response: (a) {200} grain family; (b) {220} grain family.
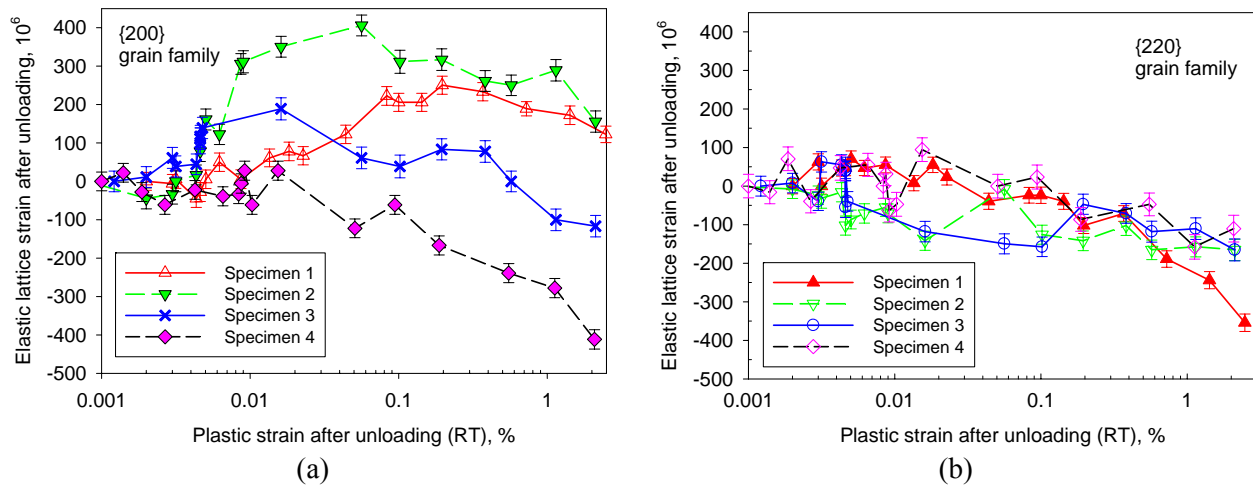

(a)   (b)

Figure 5. ND measured elastic lattice strain after each step of unloading, measured at a stress of 5MPa, plotted against the accumulated plastic strain at room temperature: (a) {200} grain family; (b) {220} grain family

3.2. Internal stress

Figs. 6 (a) and (b) show the internal stresses along the axial and radial directions for specimens subjected to prior deformation.   In general, an increase in the magnitude of the prior strain led to a higher internal stress.   In addition, the internal stress was shown to have a crystallographic orientation dependence: internal stress in {200} grain family was tensile, whereas the other three were compressive.   Of the three grain families the {220} grain family contained the highest compressive internal stress.   Rietveld refinement predicted an averaged value for four grain families considered in Figs. 6 (a) and (b).   It is interesting to note that {200} grain family in specimen 4 (highest total true axial strain) had a very similar value of internal stress compared with specimen 3.   However, the {220} grain family in specimen 4 had an increased value of internal stress compared with specimen 3.   These two phenomena are consistent with the in-situ observations shown in Fig. 4 (a) and (b), where a very similar lattice strain response was observed in the {200} grain family from specimens 3 and 4; this is different for the {220} grain family.
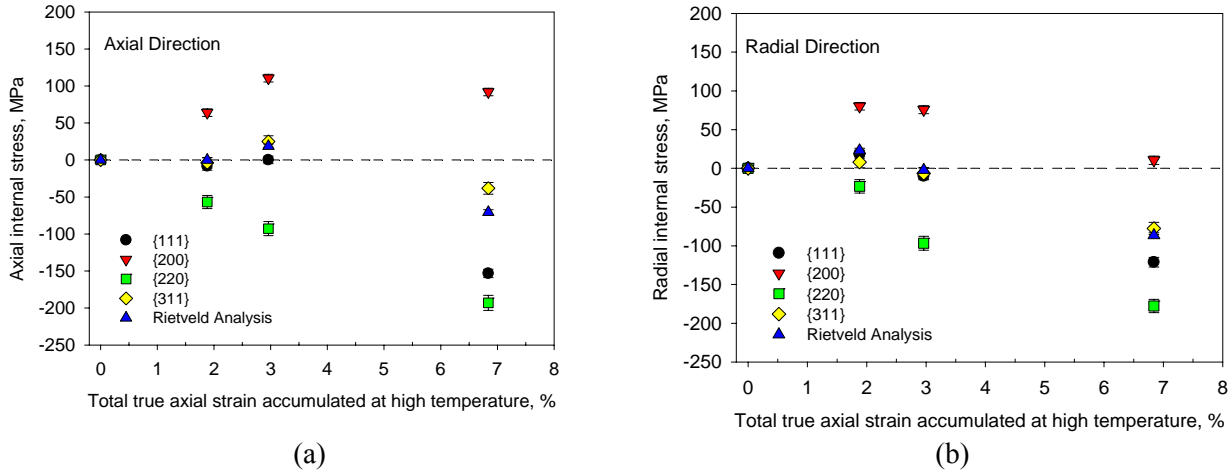
Figure 6. Internal stresses in specimens 1 to 4, which were subjected to a prior deformation at high temperature: (a) axial direction and (b) radial direction

3.3. Internal resistance

Using the incremental tensile deformation for each specimen combined with neutron diffraction measurements, the magnitude of applied stress required to create room temperature plastic deformation was obtained. This is judged to be a measure of the internal resistance to material flow. Fig. 7 shows the internal resistance in the four specimens summarised in Table 2. Internal resistance obtained from the bulk stress-strain, {220} grain family is shown in Fig. 7. Here, the 0.01% plastic strain is used as a benchmark to determine the yield point for both macro-scale and grain family size-scale conditions. The internal resistance was determined using:

$$\sigma_{bulk}^{ir} = \sigma_a^{0.01\%, bulk} \tag{5}$$

$$\sigma_{220}^{ir} = \sigma_a^{0.01\%, \{220\}} \tag{6}$$

$$\sigma_{220}^{ir} = E_{220} \times \varepsilon_{220}^{0.01\%} \tag{7}$$

Equation 5 provides a measure of the macro-scale internal resistance, σ_{bulk}^{ir}, and was determined from the applied stress required to introduce 0.01% macro-scale plastic strain. Equation 6 provides a measure of the grain family size-scale internal resistance, σ_{220}^{ir}, determined from the applied stress that is required to introduce 0.01% micro-scale plastic strain. This is the deviation calculated in Fig. 4 (b). Equation 7 provides a second choice to measure σ_{220}^{ir}, determined from the 0.01% micro-scale plastic strain, using the DEC for {220} grain family given in Table 3.
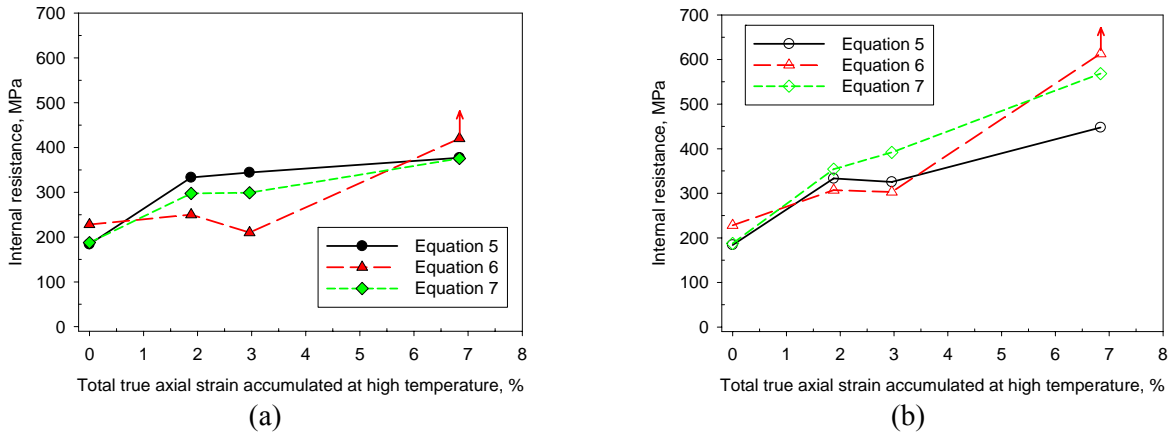

Figure 7. Internal resistance in specimens subjected to prior deformation at high temperature: (a) internal resistance without knowledge of internal stress; (b) internal resistance with knowledge of internal stress

The evaluation of internal resistance without the knowledge of the pre-existing internal stress due to the prior high temperature deformation is shown in Fig. 7 (a). The combination of ND measured internal stresses in section 3.2 and the determined internal resistance produces the correct magnitude of the internal resistance, Fig. 7 (b). The internal stresses determined via Rietveld refinement was used to correct the macro-yield strength, read from each bulk stress-strain curve for the corresponding specimens. In general, the internal resistance of the material increased with an increase in the level of the prior strain induced at high temperature. The points with an upper arrow in Fig. 7 (a) and (b) indicates that the {220} grain family did not yield with the applied stress, as shown by specimen 4 in Fig. 4 (b).

4. Discussion and Concluding Remarks

Internal stress is a consequence of strain incompatibility between grains which deform differently due to their specific orientation. This deformation, arising from slip on {111} <110> system, is accommodated elastically within the various crystallographic grain families. Internal resistance is a reflection of the material internal microstructure that resists plastic deformation. These two terms have been measured using the present ND technique and the success is attributed to the separation of internal stress and internal resistance. The former can be measured after unloading from high temperature deformation by using a microstructure freezing technique. The latter can be measured with the applied stress to evaluate the flow stress. Mecking and Kocks [15], and Follansbee and Kocks [16] proposed a model and experimental method to measure the internal resistance (called a threshold strength) at temperatures of <300K. However, in this case the presence of the internal stress was not taken into account when the internal resistance was determined. The technique proposed in this paper measures the internal resistance and internal stress at both macro-scale and at the scale of grain families. The latter is very important when providing a crystal plasticity based self-consistent model, see Ref [12].

Using this approach it is found that the internal stress is dependent on the specific crystallographic orientation of each grain family, as shown in Fig. 6. The increase in the magnitude of the internal stress, {200} in tension and {220} in compression, corresponds to the increase in the inhomogeneous strain induced by high temperature deformation, summarised in Table 2. High temperature recovery may play a role in accommodating the strain incompatibility, and lead to a small decrease in the measured internal stress, see {200} grain family for specimens 3 and 4 shown in Fig. 6. This indicates that the creep deformation rate is grain orientation dependent, otherwise the accommodation will not decrease strain incompatibility in a polycrystalline material.

The crystallographic orientation dependence of the elastic lattice strain on the applied stress, Fig. 3 (a), is consistent with a previous study by Daymond and Bouchard [17]. The present work specifically explored the influence of the prior deformation at high temperature on the measured elastic lattice strain. It was shown that the {220} grain family no longer yielded after secondary creep deformation, see specimen 4 in Fig. 4 (b). The residual lattice strain, measured after each unloading step of the incremental tensile deformation, revealed a strong influence of creep deformation on the ability of the material to plastically deform in the {220} and {200} grain families, Fig. 5 (a) and (b).

Finally, we have described a method to distinguish between the internal stress and internal resistance based on neutron diffraction measurements combined with in-situ incremental deformation. This could be used to validate the threshold strength concept, proposed by Kocks, Mecking and their co-workers [9, 15, 16]. This has been discussed more fully in a review by Kocks and Mecking [18].

Acknowledgements

References

[1] H.J. Frost, M.F. Ashby, Deformation-mechanism Maps, Pergamon, Exeter, 1982.

[2] D.G. Morris, Creep in Type 316 stainless steel, Acta Metall., 26 (1978) 1143-1151.

[3] D.G. Morris, D.R. Harries, Metal Sci., 12 (1978) 525-531.

[4] M. Biberger, J.C. Gibeling, Analysis of creep transients in pure metals following stress changes, Acta Metall. Mater., 43 (1995) 3247–3260.

[5] B. Chen, P.E.J. Flewitt, D.J. Smith, A.C.F. Cocks, A review of the changes to internal state related to high temperature creep of polycrystalline metals and alloys, Int. Mater. Rev., (to be published).

[6] C.N. Ahlquist, W.D. Nix, The measurement of internal stresses during creep of Al and Al-Mg alloys, Acta Metall., 19 (1971) 373-385.

[7] S. Straub, W. Blum, H.J. Maier, T. Ungar, A. Borbely, H. Renner, Long-range internal stresses in cell and subgrain structures of copper during deformation at constant stress, Acta Mater., 44 (1996) 4337-4350.

[8] M.A. Morris, J.L. Martin, Microstructural dependence of effective stresses and activation volumes during creep, Acta Metall., 32 (1984) 1609-1623.

[9] Y. Estrin, H. Mecking, A unified phenomenological description of work hardening and creep based on one-parameter models, Acta Metall., 32 (1984) 57-70.

[10] B. Derby, M.F. Ashby, A microstructural model for primary creep, Acta Metall., 35 (1987) 1349-1353.

[11] L. Esposito, N. Bonora, A primary creep model for class M materials, Mater. Sci. Eng. A 528 (2011) 5496-5501.

[12] J.N. Hu, B. Chen, D.J. Smith, A.C.F. Cocks, A self-consistent model in the local residual stress evaluation of 316H stainless steel, 13th Int. Conf. Fract., Beijing, (2013).

[13] J.R. Santisteban, M.R. Daymond, J.A. James, L. Edwards, ENGIN-X: a third-generation neutron strain scanner, J. Appl. Cryst. 39 (2006) 812-825.

[14] M.R. Daymond, M.A.M. Bourke, R.B. Von Dreele, B. Clausen, T. Lorentzen, Use of Rietveld refinement for elastic macrostrain determination and for evaluation of plastic strain history from diffraction spectra, J. Appl. Phys., 82 (1997) 1554-1562.

[15] H. Mecking, U.F. Kocks, Kinetics of flow and strain hardening, Acta Metall., 29 (1981) 1865-1875.

[16] P.S. Follansbee, U.F. Kocks, A constitutive description of the deformation of copper based on the use of the mechanical threshold stress as an internal state variable, Acta Metall. 36 (1988) 81-93.

[17] M.R. Daymond, P.J. Bouchard, Elastoplastic deformation of 316 stainless steel under tensile loading at elevated temperatures, Metall. Mater. Trans. A 37 (2006) 1863-1873.

[18] U.F. Kocks, H. Mecking, Physics and phenomenology of strain hardening: the FCC case, Prog. Mater. Sci. 48 (2003) 171-273.